CrystEngComm

ROYAL SOCIETY OF CHEMISTRY

PAPER

View Article Online
View Journal | View Issue

Check for updates

Cite this: *CrystEngComm*, 2022, **24**, 6349

Hidden ordered structure in the archetypical Fe(pyrazine)[Pt(CN)$_4$] spin-crossover porous coordination compound†

Ángel Fernández-Blanco,[ab] Lorenzo A. Mariano,[b] Lucía Piñeiro-López,[c] José Antonio Real,[d] Jose Sanchez Costa,[c] Roberta Poloni *[b] and J. Alberto Rodríguez-Velamazán *[a]

Received 1st July 2022,
Accepted 26th July 2022

DOI: 10.1039/d2ce00895e

rsc.li/crystengcomm

Despite the fact that Fe(pyrazine)[M^{II}(CN)$_4$] (where M^{II} is a metal in an open square-planar configuration, namely Pt, Pd, and Ni) is one of the most thoroughly studied families of spin-crossover compounds, its actual structure has remained imprecisely known up to now. Using neutron diffraction and density-functional theory calculations, we demonstrate that the pyrazine rings, instead of being disordered in two orthogonal positions in the low-spin phase, adopt an ordered arrangement with the rings alternately oriented in these two positions. This finding has a direct implication on the most characteristic property of these systems, the spin-crossover transition, which is notably affected by this arrangement. This is because the energy difference between both spin states depends on the pyrazine configuration and the ordering of the rings changes the balance of entropy contributions to the entropy-driven spin-crossover phenomenon.

1 Introduction

Coordination chemistry has experienced a remarkable surge in the last few years largely due to the burgeoning of metal–organic frameworks (MOFs), a topic where the structure–property correlation plays a crucial role. Evidently, X-ray diffraction is an essential tool in this research field, but it has some limitations that may be overcome with other techniques. In this line, neutron diffraction is a powerful complement, in particular for cases where hydrogen positioning is important, since it gives information that can be essential, as we illustrate in this work.

A new field opened for spin-crossover (SCO) materials[1] when bistability provided by the SCO phenomenon was combined with porosity in a porous coordination polymer (PCP) or a MOF.[2] This combination opened a vast playground of possibilities for applications in fields like gas capture[3] or chemical sensing,[4] since SCO can both modulate the interaction with a guest molecule and be modulated by the interaction with an adsorbed molecule.[5–9] An archetypical example of this class of compounds is the family Fe(pyrazine)[M^{II}(CN)$_4$] (where M^{II} is a metal in an open square-planar configuration, namely Pt, Pd, and Ni).[10,11] Based on classical Hofmann clathrate compounds,[12] these three-dimensional frameworks present, together with the mentioned combination of porosity and SCO,[13,14] an extremely rich display of functional properties. These include, for example, chemo-[15–17] and photo-switching,[18–20] molecular rotation correlated with the change of spin state,[21] and pressure-tunable bistability.[22] Inspired by this approach, many other examples have followed, aiming at enhancing the porosity,[23] the cooperativity and loading capacity,[24] and the interplay between the host–guest function and the SCO.[25] The structure of Fe(pyrazine)[M^{II}(CN)$_4$] adopts a general topology consisting of 2D {Fe[M^{II}(CN)$_4$]}$_\infty$ layers, with the pyrazine ligands occupying the apical positions of Fe octahedra and connecting the layers along the perpendicular direction (Fig. 1). Three possible configurations can be contemplated for the orientation of the pyrazine rings in a layer (Fig. 1): the molecules in a parallel configuration, in a perpendicular configuration in two positions 90° from each other, and orientationally disordered in these two positions (disordered configuration). It is generally assumed that the pyrazine rings are orientationally disordered, with this disorder being dynamic in the high-spin (HS) state and nearly static in the low spin (LS) state.[21] Initially, the tetragonal space group

[a] *Institut Laue Langevin, 71 Avenue des Martyrs, CS 20156-38042Grenoble, France. E-mail: velamazan@ill.eu*
[b] *Univ. Grenoble Alpes, SIMaP, Grenoble-INP, CNRS, F-38042, Grenoble, France. E-mail: roberta.poloni@grenoble-inp.fr*
[c] *IMDEA Nanociencia, Faraday 9, Ciudad Universitaria de Cantoblanco, 28049, Madrid, Spain*
[d] *Departamento de Química Inorgánica, Insituto de Ciencia Molecular (ICMol), Universidad de Valencia, 46980, Paterna, Spain*

† Electronic supplementary information (ESI) available. See DOI: https://doi.org/10.1039/d2ce00895e

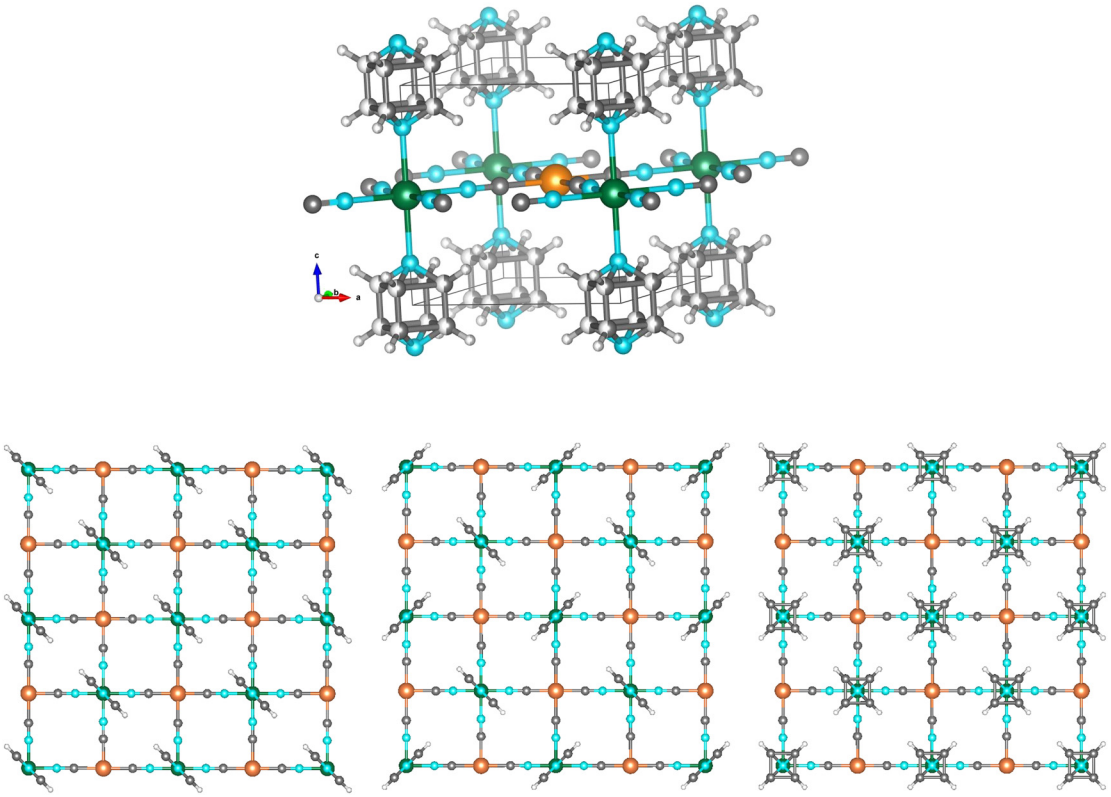

Fig. 1 (Top) Scheme of the crystal structure of Fe(pyrazine)[$M^{II}(CN)_4$] with the pyrazine rings in a disordered configuration: Fe (green), M^{II} (orange), N (light blue), C (dark grey), H (light grey). The unit cell is represented by the black lines. (Bottom) Representations of the three possible configurations of the pyrazine bridges: in a parallel configuration, in a perpendicular configuration and in a disordered configuration. Details of the structural parameters used for depicting these structures are given in the ESI.†

*P*4/*m*, which implies a disordered configuration due to the 4-fold axis passing through the N atoms of the pyrazine, was proposed from structural determination based on PXRD data.[10] Later, single-crystal X-ray diffraction studies allowed the assignation of the *P*4/*mmm* space group (also implying a disordered configuration),[13,15–17,26] which has been thoroughly assumed in subsequent studies for these compounds in both spin states in the absence of host molecules. Interestingly, Southon *et al.*[13] pointed to a parallel configuration upon incorporation of two water molecules per unit cell. They found a twinned structure with the orthorhombic space group *Pmmm*, with the pyrazines parallel within each twin, but with a 50 : 50 occupation of both possible orthogonal orientations. In the same work, the authors reported also an intermediate partially dehydrated phase, with one water molecule in the cavities presenting a perpendicular configuration of the pyrazine rings characterized by the appearance of superstructure peaks. The disordered configuration was nevertheless retained for the apohost.

In this work, we use neutron diffraction to demonstrate that the pyrazine rings adopt the perpendicular configuration in the LS state in the guest-free Fe(pyrazine)[$Pt^{II}(CN)_4$] compound, contrary to what has been generally assumed before. This observation is fully confirmed by density-functional theory calculations performed on the two configurations. Finally, the consequences of the pyrazine ordering on the spin crossover transition temperature are discussed based on the effect on the computed energy and entropy contributions. These findings have important implications because the number of studies dedicated to this family is huge owing to the vast panoply of remarkable properties these compounds present.

2 Results and discussion

2.1 Neutron diffraction

The structure of the generally accepted disordered configuration is described in the *P*4/*mmm* tetragonal space group with cell parameters $a = b = 7.33(3)$ Å and $c = 6.94(2)$ Å for the low-spin state.[15] The perpendicular configuration implies instead a structural transformation to a tetragonal supercell with $\mathbf{a}'' = \mathbf{a} - \mathbf{b}$, $\mathbf{b}'' = \mathbf{a} + \mathbf{b}$, and $\mathbf{c}'' = \mathbf{c}$, giving $a'' = b'' \approx \sqrt{2}a$ and $c'' \approx c$.[13] This transformation may therefore involve the emergence of superstructure diffraction peaks. However, when working with X-rays, these peaks are weak and can be overlooked, particularly in powder diffraction. Additionally, these superstructure reflections can be diffuse, because the orientation of the rings may be uncorrelated between layers along *c*.[13] The contrast provided by neutrons

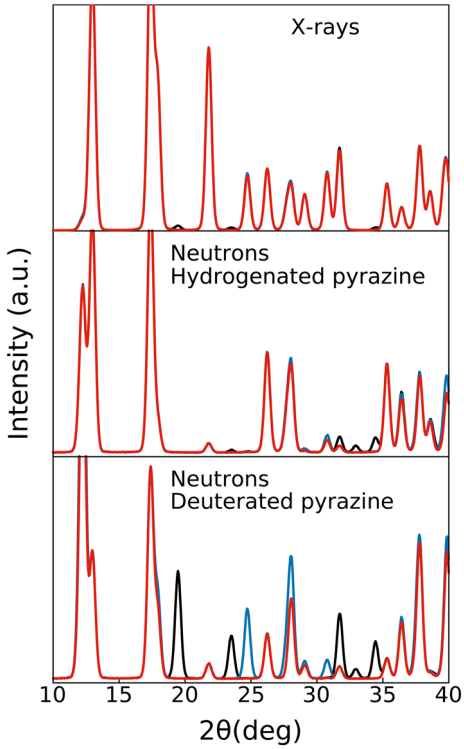

Fig. 2 Simulated powder diffraction patterns (wavelength 1.54 Å) of Fe(pyrazine)[Pt(CN)$_4$] in the low-spin state with the pyrazine rings in the disordered configuration (red lines), and in the ordered perpendicular (black lines) and parallel (blue lines) configurations: (top) X-rays and hydrogenated pyrazine; (middle) neutrons and hydrogenated pyrazine; (bottom) neutrons and deuterated pyrazine. Details of the parameters used in the simulation are given in the ESI.†

for light atoms (like hydrogen in the pyrazine molecule) allows distinguishing between the possible configurations of the rings, particularly if hydrogen is replaced by the more coherent scatterer deuterium (Fig. 2). We note that the parallel configuration, with the same cell parameters as the disordered configuration but with the space group *Pmmm*,[15] is also clearly distinguishable when using neutron diffraction on the deuterated compound (Fig. 2).

Dehydrated microcrystalline Fe(pyrazine)[Pt^{II}(CN)$_4$] and its d_4 pyrazine homologue Fe(d_4-pyrazine)[Pt^{II}(CN)$_4$] were prepared as described elsewhere.[10,15–17] Neutron diffraction experiments were performed on powder samples of *ca.* 0.25 g using the D20 instrument[27] at Institut Laue-Langevin, Grenoble, France, equipped with a cryo-furnace and using a wavelength of 1.54 Å coming from a germanium monochromator. Rietveld refinements and calculations of the structures were performed using the FullProf suite of programs[28,29] and the tools from the Bilbao Crystallographic Server.[30]

The neutron diffraction results are shown in Fig. 3 and Table 1. Fig. 3a shows the neutron diffraction pattern of Fe(d_4-pyrazine)[M^{II}(CN)$_4$] at 100 K (low-spin state). At 2θ = 19.5, 23.7 and 34.7 degrees, the superstructure reflections appearing due to the pyrazine ordering in the perpendicular configuration can be clearly observed. The experimental pattern agrees well with a model with the pyrazine rings in the perpendicular configuration, described in the supercell defined above, with the tetragonal space group *P*4/*mbm*[13] presenting a 4-fold axis passing through the Pt atom. We note that the real symmetry is probably lower, but the tetragonal pseudosymmetry avoids overparametrization. The fit is slightly improved if some disorder is allowed between both perpendicular positions of the pyrazine – with a refined value of 17.4(3)%. This is consistent with some degree of orientational disorder and with defects in the correlation of the layers along *c*.

The ordering in the perpendicular configuration of the pyrazine bridges is concomitant with the spin transition. The recorded diffraction patterns upon cooling from 320 K to 245 K (Fig. 3b) show the appearance of the superstructure reflections at the same temperature (*ca.* 285 K) of the abrupt change in the whole pattern occurring at the transition. The perpendicular configuration is the most stable at low temperatures (see below) and in fact, it has been observed in similar compounds not displaying spin-crossover.[31] However, in the present case, it occurs concurrently with the abrupt structural changes produced at the spin transition. It deserves to be noted that the perpendicular configuration is also the one found compatible with the experimental results and calculations when certain types (and quantities) of molecules are adsorbed.[13,32] In the high-spin state, the diffractogram does not show any signal of superstructure reflections and can be satisfactorily fitted with the disordered model with the space group *P*4/*mmm* (Fig. 3c). It is worthy to note that the ordering of the pyrazine molecules in the low-spin state is not an effect of the deuteration. Indeed, although less visible than those in the deuterated compound, the diffraction patterns measured for the hydrogenated compound in the low-spin state (Fig. 3d) also show evidence of pyrazine ordering (see the superstructure reflections at 2θ = 34.6 degrees).

2.2 Pyrazine interaction

In order to understand the greater stability of the perpendicular configuration, we have performed DFT calculations using the Quantum ESPRESSO package.[33,34] The PBE+D2 functional[35,36] was used to compute the binding energy of three different pyrazine dimers that represent the possible configurations present in the system: i) perpendicular, ii) top-on and iii) side-to-side dimers for the parallel arrangement (see inset in Fig. 4). See computational details in the ESI† for more details.

Taking the positions and structures of the pyrazine rings from the corresponding relaxed compound as the starting point, one of the monomers was moved along the axis that connects the centers of mass of the two molecules until a local minimum was reached. The potential energy curves obtained for the three configurations are presented in Fig. 4. The three minima were found at center-to-center distances

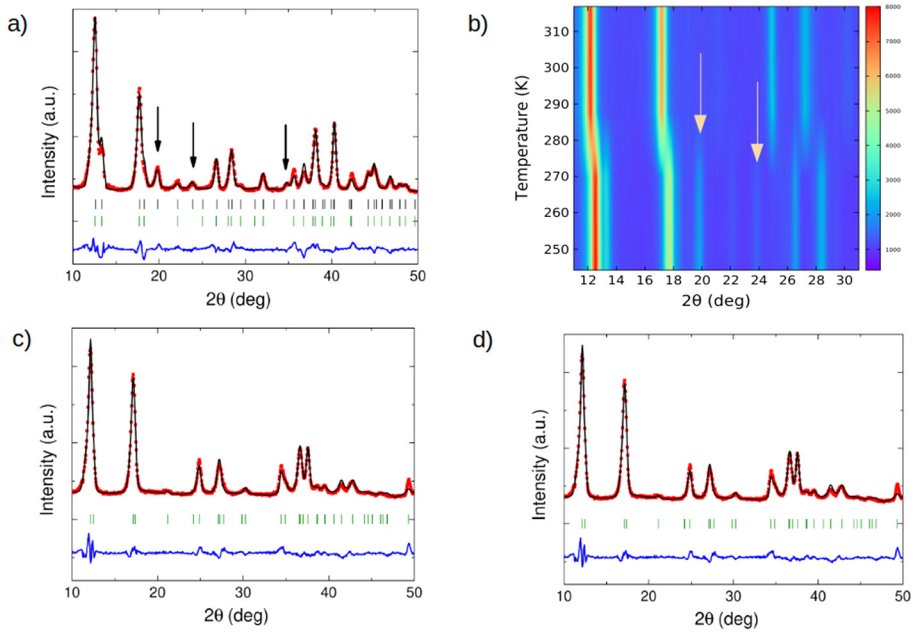

Fig. 3 Details of the most relevant part of the powder neutron diffraction patterns (wavelength 1.54 Å) of Fe(d_4-pyrazine)[Pt(CN)$_4$] (a and c) and Fe(pyrazine)[Pt(CN)$_4$] (d): experimental patterns (red), calculated patterns (black), difference patterns (blue lines), and position of the Bragg reflections for the disordered configuration (green marks) and the ordered arrangement of the pyrazine bridges in perpendicular configuration (black marks). The arrows indicate the observed superstructure reflections related to the ordering of the pyrazine bridges in the perpendicular configuration. Panel a) Fe(d_4-pyrazine)[Pt(CN)$_4$] in the low-spin state (100 K). Panel b) neutron thermodiffractograms collected upon cooling from 320 K to 245 K (cooling rate *ca.* 1.5 K min^{-1}, acquisition every 5 minutes) for Fe(d_4-pyrazine)[Pt(CN)$_4$]. Panel c) Fe(d_4-pyrazine)[Pt(CN)$_4$] in the high-spin state (320 K). Panel d) Fe(pyrazine)[Pt(CN)$_4$] in the low-spin state (130 K).

($R_{centers}$) between pyrazines of 4.8 Å, 3.8 Å, and 6.4 Å for the perpendicular, top-on, and side-to-side dimers, respectively. We note that the distance between complexed pyrazines in the framework is 7.1 Å, which is significantly larger than any of the $R_{centers}$ values and falls almost at the end of the potential energy curves (see circles on the curves in Fig. 4). An attractive interaction is predicted nonetheless for every configuration at $R_{centers}$ = 7.1 Å, being E_{int} = −11.1 meV and E_{int} = −6.7 meV for the perpendicular and side-to-side configurations, respectively, and negligible (E_{int} = −0.2 meV) for the top-on dimer. By adding up the side-to-side and top-on energy contributions, we obtain a lower value than the interaction predicted for the perpendicular configuration. This simple dimer model therefore suggests a perpendicular configuration of pyrazines for molecules located at the same distance found in the clathrate.

We note the unusual shape of the potential energy curve of the side-to-side configuration where two different regions can be found: a stabilization region between 6.1 Å and 7.6 Å and a destabilization region for $R_{centers}$ > 7.6 Å. The first

Table 1 Results of the refinement of the powder neutron diffraction patterns of Fe(d_4-pyrazine)[Pt(CN)$_4$] and Fe(pyrazine)[Pt(CN)$_4$]: the space group, cell parameters, selected distances and agreement factors are reported in each case

Compound	Fe(d_4-pyrazine)[Pt(CN)$_4$]		Fe(pyrazine)[Pt(CN)$_4$]	
T (K)	100	320	130	320
Spin state	Low-spin	High-spin	Low-spin	High-spin
Space group	*P*4/*mbm*	*P*4/*mmm*	*P*4/*mbm*	*P*4/*mmm*
a, b (Å)	10.1568(4)	7.4285(8)	10.1576(5)	7.4299(3)
c (Å)	6.7632(5)	7.2316(7)	6.7668(4)	7.2369(5)
$d_{(Fe–N(C))}$ (Å)	1.903(5)	2.1599(3)	1.941(5)	2.1583(2)
$d_{(Fe–N(pz))}$ (Å)	1.983(7)	2.2273(3)	1.978(7)	2.2291(3)
R_{Bragg}	5.69	7.70	5.03	8.81

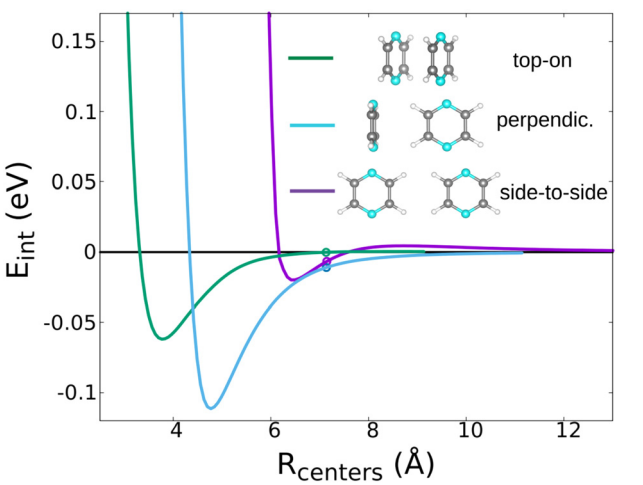

Fig. 4 Interaction energy, E_{int}, computed for the three pyrazine dimers: top-on (green), perpendicular (light blue), and side-to-side (purple). The *x*-axis ($R_{centers}$) gives the center-to-center distance between pyrazine moeities. The circles indicate the distance at which pyrazines are found in the Hofmann clathrate, *i.e.* $R_{centers}$ = 7.1 Å.

corresponds to d(H–H) between 2.1 and 3.4 Å which correlates with the typical formation distances of a H–H bond.[37,38] This weak bond with a dispersive nature exhibits energies of the order of 0.017 eV, comparable to the maximum stabilization of 0.020 eV predicted at the equilibrium position in Fig. 4. For $R_{centers} > 7.6$ Å, the H–H distance is too large for a typical H–H bond and the electrostatic repulsion between the pyrazines may dominate. Finally, this analysis is consistent with the (PBE+D2) computed total energy difference between the parallel and perpendicular configurations in the supercell which gives a more stable perpendicular case by 35 meV per pyrazine.

2.3 Influence of the pyrazine arrangement on the spin transition

The configuration of the pyrazine rings has important consequences for the most characteristic feature of this material: the spin-crossover transition.

It is not unusual to observe order–disorder processes coupled to SCO.[39,40] In most cases, it is related to counterions or solvent molecules present in the structure,[41,42] and more rarely to ligands.[43,44] An order–disorder process can affect the spin transition in several ways, including the temperature of the transition and its abruptness (and hysteresis), and this has been taken into account in theoretical models of the spin transition.[45] When coupling exists between the spin-active part of the system and the moieties susceptible of undergoing order–disorder, the presence of order–disorder processes tends to increase the abruptness of the transition, as has been observed in different examples.[46–48] The wide hysteresis observed in Fe(pyrazine)[Pt(CN)$_4$] may be therefore related to the order–disorder process undergone by the pyrazine rings.

Particularly relevant is how the pyrazine arrangement significantly affects the transition temperature. The spin transition temperature, $T_{1/2}$, from LS to HS is defined as the temperature at which the thermodynamic equilibrium between the two phases is reached, *i.e.* when the Gibbs free energy is zero. The transition temperature is then given by $T_{1/2} = \Delta H_{HS-LS}/\Delta S_{HS-LS}$, with ΔH_{HS-LS} (ΔS_{HS-LS}) being the enthalpy (entropy) difference between both spin states. The experimental values for these quantities are ΔH_{exp} = 25 kJ mol^{-1} and ΔS_{exp} = 84 J mol^{-1} K^{-1} (giving $T_{1/2}$ = 297 K).[11] Both the energy and entropy differences depend on the configuration of the pyrazine rings, and therefore the transition temperature would be substantially modified if the pyrazine arrangement was different. The different terms contributing to ΔH_{HS-LS} and ΔS_{HS-LS}, and thus to $T_{1/2}$, are written in eqn (1)

$$T_{1/2} = \frac{\Delta H_{HS-LS}}{\Delta S_{HS-LS}} = \frac{\Delta E_{ad} + \Delta E_{vib}}{\Delta S_{vib} + \Delta S_{rot} + \Delta S_{el}} \quad (1)$$

The enthalpy difference, ΔH_{HS-LS}, contains two terms, the adiabatic energy difference, ΔE_{ad}, and the vibrational contribution, ΔE_{vib}. The entropy variation, ΔS_{HS-LS}, contains the vibrational contribution, ΔS_{vib}, a rotational term, ΔS_{rot}, which accounts for the degrees of freedom associated with the rotational motion of the pyrazine rings,[21] and an electronic contribution, ΔS_{el}, which takes into account the different spin multiplicities between the two spin states. In the case of a LS–HS transition in Fe(II) complexes between a LS state with S = 0 and a HS state with S = 2, ΔS_{el} = 13.38 J mol^{-1} K^{-1}. This term, which represents *ca.* 16% of the entropy variation at the transition, is independent from the arrangement of the pyrazine rings.

ΔS_{rot} is instead significantly affected by the pyrazine configuration. In 2012, a study of the dynamics of this system by some of us demonstrated, by means of quasielastic neutron scattering – a technique particularly adapted to probe the movement of hydrogen atoms – that the pyrazine rings are rotating in HS, while in LS, the movement is virtually deactivated.[21] The rotational term ΔS_{rot} was thereby calculated to amount to 7.95 J mol^{-1} K^{-1} (ref. 21) (*ca.* 9.4% of the total entropy gain at the transition) assuming a LS state with the pyrazine rings disordered in two perpendicular positions. Because the pyrazine molecules are ordered in LS, as demonstrated in the present neutron diffraction study, the number of accessible positions is divided by two, and so does the entropy. This leads to a change in ΔS_{rot} of at least a factor of two (under the approximation of a harmonic oscillator around its equilibrium position, which is the case with less entropy, and therefore less favorable to produce big differences when applying a factor of two to it). A difference of this magnitude in ΔS_{rot} between the LS-ordered case and the LS-disordered one implies a decrease of *ca.* 10% of the total experimental entropy obtained for the title compound.

We performed DFT calculations to compute how the pyrazine configuration affects the other terms such as E_{ad}, E_{vib} and S_{vib}. For this, we computed the total energy and normal modes for the compound with the pyrazine rings in perpendicular and parallel configurations in both the HS and LS states. We take the average of the perpendicular and parallel cases as an approximation for the disordered case (see the full set of values in Table S2 in the ESI†). The expression for the vibrational contributions E_{vib} and S_{vib} can be derived within the statistical thermodynamic theory from the partition function of a harmonic oscillator. For a given normal mode vibrational spectrum $\{\nu_i\}$, the vibrational contributions are:

$$E_{vib} = R\sum_{\nu_i}\frac{h\nu_i}{k_B}\left(\frac{1}{2} + \frac{1}{e^{h\nu_i/k_BT}-1}\right) \quad (2)$$

and

$$S_{vib} = R\sum_{\nu_i}\left(\frac{h\nu_i}{k_BT}\frac{1}{e^{(h\nu_i/k_BT)}-1} - \ln\left(1-e^{-h\nu_i/k_BT}\right)\right) \quad (3)$$

The DFT results show a difference of 0.83 J mol^{-1} K^{-1} in ΔS_{vib} (*ca.* 1% of the total experimental entropy gain at the

transition) between a LS-ordered case and a fully disordered scenario. The LS-ordered case consists of the difference between a disordered HS state and an ordered LS state with a perpendicular arrangement. The fully disordered case consists of disordered configurations both in the HS and LS states. Regarding ΔE_{vib}, a negligible difference of 0.02 kJ mol^{-1} (less than 0.1% of the total enthalpy variation at the transition) is computed.

Finally, the adiabatic energy difference, ΔE_{ad}, is computed as the total energy difference between the two spin states each taken at their corresponding geometry. We note that the calculation of adiabatic energy differences in transition metal complexes presents a significant challenge for modern electronic structure methods.[49–53] Within DFT, different exchange and correlation functionals including semilocal, meta-GGAs, and global hybrids have been tested in this respect and variations by up to 3 eV can be found depending on the specific choice of the functional and the chosen molecular complex.[54] Here, to evaluate ΔE_{ad}, we use the non-self consistent Hubbard U-corrected density approach scheme which employs linear response U[55] values computed separately for high spin and low spin (see the ESI† for more details). Recently, this method has been shown to provide accurate results of spin splitting energies for a series of Fe(II) molecules and periodic compounds when compared with higher level calculations and experimentally extracted results.[53] The adiabatic energy difference computed with this method is 36.64 kJ mol^{-1} when both spin states are disordered and 36.91 kJ mol^{-1} when the LS state is in the perpendicular arrangement. This gives, as expected, a marginal energy difference of 0.27 kJ mol^{-1} between the two pyrazine configurations.

Adding together all the contributions (see eqn (1)), we obtain that the change in the configuration of pyrazine moieties in the LS state from an ordered perpendicular arrangement to a disordered case implies a decrease of 0.29 kJ mol^{-1} in ΔH and of 8.78 J mol^{-1} K^{-1} in ΔS at the spin transition, which translates in a variation of $T_{1/2}$ of the order of 30 K. Thus, if the configuration of the pyrazine rings in the LS state was disordered and not ordered, the transition temperature would have been *ca.* 30 K higher, mostly due to the change in rotational entropy.

3 Conclusion

Herein, we have demonstrated, by means of neutron diffraction experiments, that the pyrazine rings in Fe(pyrazine)[Pt(CN)$_4$] adopt an ordered arrangement in the low-spin state with the rings alternately oriented in two positions perpendicular to each other. Our DFT calculations have shown that this configuration stems from the interaction between the pyrazine molecules and have allowed us to estimate the effect of this arrangement at the spin transition temperature. The implications of the actual configuration of the pyrazine moieties in the energy and entropy balance between the high-spin and low-spin states are substantial, and thus the spin transition temperature is significantly dependent on this configuration. The fact that Fe(pyrazine)[M^{II}(CN)$_4$] (M^{II} = Pt, Pd, Ni) are prototypical examples of the growing class of porous spin-crossover compounds, with a relevant potential for applications, and the great number of studies concerning this family and many other compounds based on it, underlines the significance of accurate structural knowledge, which may be of crucial importance for the understanding of the properties of such materials.

Data availability

ILL beamtime allocation experiment numbers 5-22-795 (**https://doi.ill.fr/10.5291/ILL-DATA.5-22-795**) and DIR-274 (**https://doi.ill.fr/10.5291/ILL-DATA.DIR-214**).

Conflicts of interest

There are no conflicts to declare.

Acknowledgements

We thank the ILL for the PhD contract of A. F. B. and for the beamtime allocation under experiment numbers 5-22-795 and DIR-274. J. S. C. acknowledges funds from the MICINN through the National Research Project (PID2019-111479GB-100) and the Ramon y Cajal Research Program (RYC-2014-16866). IMDEA Nanociencia acknowledges support from the Severo Ochoa Program for Centres of Excellence in R&D (MICINN, Grant CEX2020-001039-S). J. A. R. thanks Grant PID2019-106147GB-I00 funded by MCIN/AEI. Calculations were performed using resources granted by GENCI under the CINES and TGCC grant numbers A0020907211 and A0110907211. Additionally, the froggy and Dahu platform of the CIMENT infrastructure, which is supported by the Rhone-Alpes region (GRANT CPER07 13 CIRA) and the Equip@Meso project, was employed for the calculations.

References

1 P. Gütlich and H. A. Goodwin, Spin-Crossover in Transition Metal Compounds, in *Topics in Current Chemistry*, Springer, Berlin, 2004, vol. I–III.
2 J. A. Real, E. Andrés, M. C. Muñoz, M. Julve, T. Granier, A. Bousseksou and F. Varret, *Science*, 1995, **268**, 265–267.
3 D. A. Reed, B. K. Keitz, J. Oktawiec, J. A. Mason, T. Runčevski, D. J. Xiao, L. E. Darago, V. C. Valentina, S. Bordiga and J. R. Long, *Nature*, 2017, **550**, 1476–4687.
4 G. J. Halder, C. J. Kepert, B. Moubaraki, K. S. Murray and J. D. Cashion, *Science*, 2002, **298**, 1762–1765.
5 X. Bao, H. J. Shepherd, L. Salmon, G. Molnár, M.-L. Tong and A. Bousseksou, *Angew. Chem., Int. Ed.*, 2013, **52**, 1198–1202.
6 R. Ohtani and S. Hayami, *Chem. – Eur. J.*, 2017, **23**, 2236–2248.

7 Z.-P. Ni, J.-L. Liu, M. N. Hoque, W. Liu, J.-Y. Li, Y.-C. Chen and M.-L. Tong, *Coord. Chem. Rev.*, 2017, **335**, 28–43.
8 E. Resines-Urien, E. Burzurí, E. Fernandez-Bartolome, M. A. García García-Tuñón, P. de la Presa, R. Poloni, S. J. Teat and J. S. Costa, *Chem. Sci.*, 2019, **10**, 6612–6616.
9 A. Develioglu, E. Resines-Urien, R. Poloni, L. Martín-Pérez, J. S. Costa and E. Burzurí, *Adv. Sci.*, 2021, **8**, 2102619.
10 V. Niel, J. M. Martínez-Agudo, M. C. Muñoz, A. B. Gaspar and J. A. Real, *Inorg. Chem.*, 2001, **40**, 3838–3839.
11 T. Tayagaki, A. Galet, G. Molnár, M. C. Muñoz, A. Zwick, K. Tanaka, J. A. Real and A. Bousseksou, *J. Phys. Chem. B*, 2005, **109**, 14859–14867.
12 K. A. Hofmann, F. Küspert and Z. Anorg, *Chem*, 1897, **15**, 204–207.
13 P. D. Southon, L. Liu, E. A. Fellows, D. J. Price, G. J. Halder, K. W. Chapman, B. Moubaraki, K. S. Murray, J.-F. Létard and C. J. Kepert, *J. Am. Chem. Soc.*, 2009, **131**, 10998–11009.
14 M. C. Muñoz and J. A. Real, *Coord. Chem. Rev.*, 2011, **255**, 2068–2093.
15 M. Ohba, K. Yoneda, G. Agustí, M. C. Muñoz, A. Gaspar, J. A. Real, M. Yamasaki, H. Ando, Y. Nakao, S. Sakaki and S. Kitagawa, *Angew. Chem., Int. Ed.*, 2009, **48**, 4767–4771.
16 G. Agustí, R. Ohtani, K. Yoneda, A. B. Gaspar, M. Ohba, J. F. Sánchez-Royo, M. C. Muñoz, S. Kitagawa and J. A. Real, *Angew. Chem., Int. Ed.*, 2009, **48**, 8944–8947.
17 R. Ohtani, K. Yoneda, S. Furukawa, N. Horike, S. Kitagawa, A. B. Gaspar, M. C. Muñoz, J. A. Real and M. Ohba, *J. Am. Chem. Soc.*, 2011, **133**, 8600–8605.
18 S. Bonhommeau, G. Molnár, A. Galet, A. Zwick, J. A. R. Real, J. J. McGarvey and A. Bousseksou, *Angew. Chem., Int. Ed.*, 2005, **44**, 4069–4073.
19 S. Cobo, D. Ostrovskii, S. Bonhommeau, L. Vendier, G. Molnár, L. Salmon, K. Tanaka and A. Bousseksou, *J. Am. Chem. Soc.*, 2008, **130**, 9019–9024.
20 M. Castro, O. Roubeau, L. Piñeiro López, J. A. Real and J. A. Rodríguez-Velamazán, *J. Phys. Chem. C*, 2015, **119**, 17334–17343.
21 J. A. Rodríguez-Velamazán, M. A. González, J. A. Real, M. Castro, M. C. Muñoz, A. B. Gaspar, R. Ohtani, M. Ohba, K. Yoneda, Y. Hijikata, N. Yanai, M. Mizuno, H. Ando and S. Kitagawa, *J. Am. Chem. Soc.*, 2012, **134**, 5083–5089.
22 A. Galet, A. B. Gaspar, M. C. Muñoz, G. V. Bukin, G. Levchenko and J. A. Real, *Adv. Mater.*, 2005, **17**, 2949–2953.
23 C. Bartual-Murgui, N. A. Ortega-Villar, H. J. Shepherd, M. C. Muñoz, L. Salmon, G. Molnár, A. Bousseksou and J. A. Real, *J. Mater. Chem.*, 2011, **21**, 7217–7222.
24 L. Piñeiro López, M. Seredyuk, M. C. Muñoz and J. A. Real, *Chem. Commun.*, 2014, **50**, 1833–1835.
25 M. Meneses-Sánchez, R. Turo-Cortés, C. Bartual-Murgui, I. da Silva, M. C. Muñoz and J. A. Real, *Inorg. Chem.*, 2021, **60**, 11866–11877.
26 S. Cobo, D. Ostrovskii, S. Bonhommeau, L. Vendier, G. Molnár, L. Salmon, K. Tanaka and A. Bousseksou, *J. Am. Chem. Soc.*, 2008, **130**, 9019–9024.
27 T. C. Hansen, P. F. Henry, H. E. Fischer, J. Torregrossa and P. Convert, *Meas. Sci. Technol.*, 2008, **19**, 034001.
28 J. Rodríguez-Carvajal, *Phys. B*, 1993, **192**, 55–69.
29 **https://www.ill.eu/sites/fullprof/**.
30 M. I. Aroyo, J. M. Perez-Mato, C. Capillas, E. Kroumova, S. Ivantchev, G. Madariaga, A. Kirov and H. Wondratschek, *Z. Kristallogr. - Cryst. Mater.*, 2006, **221**, 15–27.
31 J. Rodríguez-Hernández, A. Lemus-Santana, J. Ortiz-López, S. Jiménez-Sandoval and E. Reguera, *J. Solid State Chem.*, 2010, **183**, 105–113.
32 A. Fernández-Blanco, L. Piñeiro López, M. Jiménez-Ruiz, S. Rols, J. A. Real, J. A. Rodríguez-Velamazán and R. Poloni, *J. Phys. Chem. C*, 2022, **126**, 8090–8099.
33 P. Giannozzi, O. Andreussi, T. Brumme, O. Bunau, M. B. Nardelli, M. Calandra, R. Car, C. Cavazzoni, D. Ceresoli, M. Cococcioni, N. Colonna, I. Carnimeo, A. D. Corso, S. de Gironcoli, P. Delugas, R. A. DiStasio, A. Ferretti, A. Floris, G. Fratesi, G. Fugallo, R. Gebauer, U. Gerstmann, F. Giustino, T. Gorni, J. Jia, M. Kawamura, H.-Y. Ko, A. Kokalj, E. Küçükbenli, M. Lazzeri, M. Marsili, N. Marzari, F. Mauri, N. L. Nguyen, H.-V. Nguyen, A. O. de-la Roza, L. Paulatto, S. Poncé, D. Rocca, R. Sabatini, B. Santra, M. Schlipf, A. P. Seitsonen, A. Smogunov, I. Timrov, T. Thonhauser, P. Umari, N. Vast, X. Wu and S. Baroni, *J. Phys.: Condens. Matter*, 2017, **29**, 465901.
34 P. Giannozzi, O. Baseggio, P. Bonfá, D. Brunato, R. Car, I. Carnimeo, C. Carvazzoni, S. de Gironcoli, P. Delugas, F. F. Ruffino, A. Ferreti, N. Mazari, I. Timrov, A. Urru and S. Baroni, *J. Chem. Phys.*, 2020, **152**, 154105.
35 S. Grimme, *J. Comput. Chem.*, 2006, **27**, 1787–1799.
36 S. Grimme, A. Hansen, J. G. Brandenburg and C. Bannwarth, *Chem. Rev.*, 2016, **116**, 5105–5154.
37 S. J. Grabowski, *Hydrogen Bonding- New Insights*, Springer, Amsterdam, 2006.
38 D. J. Wolstenholme and T. S. Cameron, *J. Phys. Chem. A*, 2006, **110**, 8970–8978.
39 S. Pillet, *J. Appl. Phys.*, 2021, **129**, 181101.
40 A. Kashiro, K. Some, Y. Kobayashi and T. Ishida, *Inorg. Chem.*, 2019, **58**, 7672–7676.
41 C.-F. Sheu, S. Pillet, Y.-C. Lin, S.-M. Chen, I.-J. Hsu, C. Lecomte and Y. Wang, *Inorg. Chem.*, 2008, **47**, 10866–10874.
42 H. J. Shepherd, G. Tonge, L. E. Hatcher, M. J. Bryant, J. V. Knichal, P. R. Raithby, M. A. Halcrow, R. Kulmaczewski, K. J. Gagnon and S. J. Teat, *Magnetochemistry*, 2016, **2**, 9.
43 T. M. Ross, B. Moubaraki, K. S. Wallwork, S. R. Batten and K. S. Murray, *Dalton Trans.*, 2011, **40**, 10147–10155.
44 D. Rosario-Amorin, P. Dechambenoit, A. Bentaleb, M. Rouzières, C. Mathonière and R. Clérac, *J. Am. Chem. Soc.*, 2018, **140**, 98–101.
45 D. Chernyshov, N. Klinduhov, K. W. Törnroos, M. Hostettler, B. Vangdal and H.-B. Bürgi, *Phys. Rev. B: Condens. Matter Mater. Phys.*, 2007, **76**, 014406.
46 R. Kulmaczewski, E. Trzop, E. Collet, S. Vela and M. A. Halcrow, *J. Mater. Chem. C*, 2020, **8**, 8420–8429.

47 G. S. Matouzenko, A. Bousseksou, S. A. Borshch, M. Perrin, S. Zein, L. Salmon, G. Molnar and S. Lecocq, *Inorg. Chem.*, 2004, **43**, 227–236.
48 G. A. Craig, J. S. Costa, O. Roubeau, S. J. Teat and G. Aromí, *Chem. – Eur. J.*, 2011, **17**, 3120–3127.
49 M. Radoń, *Phys. Chem. Chem. Phys.*, 2019, **21**, 4854–4870.
50 L. M. L. Daku, A. Vargas, A. Hauser, A. Fouqueau and M. E. Casida, *ChemPhysChem*, 2005, **6**, 1393–1410.
51 K. Pierloot, *Int. J. Quantum Chem.*, 2011, **111**, 3291–3301.
52 A. Droghetti, D. Alfè and S. Sanvito, *J. Chem. Phys.*, 2012, **137**, 124303.
53 L. A. Mariano, B. Vlaisavljevich and R. Poloni, *J. Chem. Theory Comput.*, 2021, **17**, 2807–2816.
54 L. A. Mariano, B. Vlaisavljevich and R. Poloni, *J. Chem. Theory Comput.*, 2020, **16**, 6755–6762.
55 M. Cococcioni and S. De Gironcoli, *Phys. Rev. B: Condens. Matter Mater. Phys.*, 2005, **71**, 035105.